



# Tannin–phenolic resins: Synthesis, characterization, and application as matrix in biobased composites reinforced with sisal fibers

Elaine C. Ramires, Elisabete Frollini \*

Macromolecular Materials and Lignocellulosic Fibers Group, Institute of Chemistry of São Carlos, University of São Paulo, C.P. 780, CEP 13560-970, São Carlos, São Paulo, Brazil

## ARTICLE INFO

### Article history:

Received 1 August 2011

Received in revised form 18 November 2011

Accepted 21 November 2011

Available online 30 April 2012

### Keywords:

A. Polymer–matrix composites (PMCs)

E. Thermosetting resin

B. Fiber/matrix bond

B. Mechanical properties

## ABSTRACT

A tannin–phenolic resin (40 wt% of tannin, characterized by  $^1\text{H}$  nuclear magnetic resonance (NMR) and  $^{13}\text{C}$  NMR, Fourier transform infrared, thermogravimetry, differential scanning calorimetry) was used to prepare composites reinforced with sisal fibers (30–70 wt%). Inverse gas chromatography results showed that the sisal fibers and the tannin–phenolic thermoset have close values of the dispersive component and also have predominance of acid sites (acid character) at the surface, confirming the favoring of interaction between the sisal fibers and the tannin–phenolic matrix at the interface. The Izod impact strength increased up to 50 wt% of sisal fibers. This composite also showed high storage modulus, and the lower loss modulus, confirming its good fiber/matrix interface, also observed by SEM images. A composite with good properties was prepared from high content of raw material obtained from renewable sources (40 wt% of tannin substituted the phenol in the preparation of the matrix and 50 wt% of matrix was replaced by sisal fibers).

© 2012 Elsevier Ltd. All rights reserved.

## 1. Introduction

The growing concern with the protection of the environment allied to the reduction of fossil resources has contributed to the development of biobased materials [1]. Composites of polymeric matrix reinforced with natural fibers have emerged as an environmentally beneficial and low-cost option to the traditionally used materials [2–4]. Natural fibers have high electrical resistance and hollow cellular structure that provides good acoustic insulation properties. They are not abrasive to the mixing and molding equipments, which significantly reduce the production costs. Besides, the availability in almost all the world is an additional advantage of these fibers [4,5]. The lignocellulosic fibers also are a good, renewable, and biodegradable alternative to replace the reinforcements obtained from non-renewable resources [6–8].

Among the several lignocellulosic fibers, the sisal is one of the most used fibers due to its high mechanical strength [2,9–11]. The properties of sisal fibers, such as stiffness, hardness, and tensile strength, depend on the cellulose content, the age of the plant, and the conditions under which they were cultivated [7]. Another advantage of the sisal fiber is that it is obtained from a plant with short growing cycle, about 24 months. Brazil is the biggest worldwide producer of sisal, with the production of 85 thousand ton in 2009 [12].

The phenolic resin can be considered as one of the first polymeric products commercially produced and used in the industry [13]. Despite the centenary, the phenolic resins are still used for a range of applications, such as thermal insulation materials, adhesives, powders of molding, laminated resins, coating of surfaces, and composites [14,15]. This occurs because of its excellent properties like dimensional stability, chemical resistance, thermal stability, and its role as a flame retardant [15–17].

The raw material used in the production of phenolic resins (mainly phenol and formaldehyde) are obtained in a large scale from non-renewable sources. Thus, the substitution of these reagents by equivalent ones obtained from non-fossil sources is an interesting alternative, providing both economical and environmental benefits [9,18].

Tannins are natural products present in several plant families and have a large amount of phenolic rings in their structure [19]. Tannins are classified in two groups: hydrolysable and condensed [20]. Condensed tannins are flavonoids units with several degrees of condensation and the hydrolysable tannins are a mixture of simple phenols, with ester linkages in their structure and are susceptible to hydrolysis by the action of diluted mineral acids, alkalis, and enzymes. Condensed tannins are the most suitable for the production of phenolic resins, due to the presence of phenolic rings *di*-substituted with hydroxyl groups in its structure. These hydroxyl groups make these rings activated faced to the attack of an electrophile, similar to the formaldehyde, owing to the electron donor effect of the hydroxyl groups [21,22].

\* Corresponding author. Tel.: +55 1633739951; fax: +55 1633739952.

E-mail address: [elisabete@iqsc.usp.br](mailto:elisabete@iqsc.usp.br) (E. Frollini).

In the previous work, Frollini et al. [18] used tannin as a partial substitute of phenol in the preparation of composites reinforced with bark from the Acacia Mimosa tree (fibers and particles). The tannin used as the substitute of phenol was also extracted from the bark of the Acacia Mimosa tree, because this tree is rich in tannin. The composites showed low water absorption and high storage modulus, due to the good adhesion at the fiber/matrix interface. With scanning electron microscopy (SEM) images, it was possible to observe the diffusion of the matrix inside the fibers. The good properties showed by the composites were consequence of the compatibility between fibers and matrix, which occurred due to the presence of tannin in both matrix and fiber.

In a companion paper, Barbosa et al. [23] used the tannin–phenolic matrix in the preparation of composites reinforced with coir fibers. The composites showed intense fiber/matrix adhesion, but the impact strength value was not high, mainly due to the poor mechanical properties of the fiber. The tensile strength of coir fiber determined using dynamic–mechanical analysis (DMA) was 120 MPa. However, it is important to notice that the composites showed higher storage modulus, demonstrating improved properties when compared with the thermoset (without fibers).

Thus, considering the promising results obtained in the companion paper [23], in this study, sisal fibers were used, which have better mechanical properties compared with the coir fibers. Moreover, some parameters of the synthesis of the resin were also optimized. The tannin–phenolic resin was prepared using the condensed-type tannin, extracted from the bark of the Acacia Mimosa tree. The inverse gas chromatography (IGC) was used to evaluate the dispersive component of the surface energy and the acid–base properties of the tannin, tannin–phenolic thermoset (TPT), and sisal fibers. To evaluate the influence of the proportion of natural fibers on the properties of the composites, the tannin–phenolic resins were used to prepare composites reinforced with 30–70 wt% of sisal fibers. This assessment has great importance, because besides investigating the production of composites with better mechanical properties, the use of larger proportion of sisal fibers results in composites with higher proportion of materials obtained from natural sources. Furthermore, the tannin–phenolic matrix has natural material in its structure, the tannin, contributing considerably to the area of development of biobased composites.

To our knowledge, the approach of the global project that involves the present study, in which tannin is used in the preparation of matrices reinforced by lignocellulosics fibers, is unprecedented.

## 2. Methods

### 2.1. Materials

The sisal fibers used as reinforcement in the tannin–phenolic composites (TPC) were kindly supplied by Lwarcel (Lençóis Paulista, SP, Brazil). Before use, the sisal fibers were Soxhlet extracted with cyclohexane/ethanol (1:1, v/v) for 50 h to remove extractives such as waxes, terpenes, and fatty acids. Then, they were washed with distilled water to remove salts and low-molecular-weight sugars and dried in an air-circulated oven at 105 °C until a constant weight was reached.

The condensed tannins, extracted from the Acacia Mimosa tree, used as a partial substitute for phenol in the phenolic resin were kindly supplied by Tanac (Montenegro, RS, Brazil) and were used as received.

Formaldehyde (37%, Synth), phenol (Synth), potassium hydroxide (Synth), and resorcinol (Vetec) were used as received.

### 2.2. Tannin–phenolic pre-polymer synthesis

The pre-polymer, containing 40 wt% of tannin replacing the phenol, was synthesized using formaldehyde, phenol, tannin, and potassium hydroxide (1.38:0.6:0.4:0.06, w/w). First, tannin, formaldehyde, and potassium hydroxide were mixed under mechanical stirring, at 40 °C for 30 min. After that, phenol was added and mixed under mechanical stirring, at 40 °C for 1 h. Then, the solution was cooled to room temperature, neutralized with concentrated hydrochloric acid, and the water was eliminated under reduced pressure.

### 2.3. Thermoset and composites preparation

The thermoset and composites were prepared by mixing the tannin–phenolic resin with resorcinol, the curing accelerator agent (10:1 w/w), under mechanical stirring at 40 °C for 30 min. For composite preparation, the sisal fibers (3 cm of length, 30–70 wt% and randomly distributed) were added to the resin with resorcinol and submitted to mechanical stirring for 20 min (JVJ mixer, Pardiniho, SP, Brazil), in order to obtain an optimum impregnation of the fibers by the resin. The fibers were previously dried for 4 h in an air-circulated oven at 105 °C to remove moisture. Compression molding was carried out in a mold (300 × 140 × 5 mm) under pressure. The molding cure cycles (40 °C/0.5 h/0 kg f cm<sup>-2</sup>; 50 °C/1 h/23.8 kg f cm<sup>-2</sup>; 85 °C/1.5 h/38.08 kg f cm<sup>-2</sup>; 125 °C/2 h/38.08 kg f cm<sup>-2</sup>; 150 °C/2 h/38.08 kg f cm<sup>-2</sup>) were based on previous studies [18].

### 2.4. Characterizations

#### 2.4.1. Tannin and tannin–phenolic resin

The <sup>1</sup>H and <sup>13</sup>C NMR (nuclear magnetic resonance) spectra of tannin and tannin–phenolic resin were recorded on a Bruker AC-200 spectrometer at 300 K, in 5 mm tubes, using DMSO-d<sub>6</sub> as solvent, with 512 and 20,000 scans, respectively. The chemical shifts were referenced to the residual signal of DMSO-d<sub>6</sub> (<sup>1</sup>H δ = 2.5 ppm and <sup>13</sup>C δ = 39.52 ppm).

The Fourier transform infrared (FT-IR) spectra were recorded on a BOMEM, model MB-102, in the range of 4000–400 cm<sup>-1</sup> and with an accumulation of 20 scans to reduce noise. The tannin was mixed with dry KBr (2:200 mg) and pressed under vacuum to form the pellet. The tannin–phenolic resin was analyzed using a silicon pellet.

The thermogravimetric (TG) analyses were carried out using Shimadzu equipment, model TGA-50. The samples (8 mg) were placed in platinum pans and heated from 25 °C to 800 °C at 10 °C min<sup>-1</sup>, under synthetic air atmosphere (flow of 20 mL min<sup>-1</sup>).

The differential scanning calorimetry (DSC) analyses were performed using a Shimadzu instrument, model DSC-50. The samples (6 mg) were placed in aluminum seal pans and heated from 100 °C to 400 °C at 10 °C min<sup>-1</sup>, under synthetic air atmosphere (flow of 20 mL min<sup>-1</sup>).

#### 2.4.2. Sisal fibers

The moisture content was determined according to ABNT NBR9656 (Brazilian Technical Standards Association) by determining the percentage difference between the initial sample weight and that after 4 h drying at 105 °C.

The ash content was determined considering the percentage difference between the initial sample weight of the dried fiber (free of moisture) and that after calcination for 4 h at 800 °C.

The Klason lignin content was determined according to the modified TAPPI T13M-54 standard. This method is based on the isolation of lignin after hydrolysis of the polysaccharides (cellulose and hemicellulose) by concentrated sulfuric acid (72%).

The holocellulose (hemicellulose + cellulose) content was determined according to the TAPPI T19m-54 by selective sodium hypochlorite degradation of the lignin at 70 °C. The cellulose content was determined by selective sodium hydroxide degradation of the hemicellulose at room temperature. The hemicellulose content was obtained by taking the difference between the holocellulose and cellulose contents.

For all the previously mentioned analyses (except for moisture content), the samples were previously dried for 4 h in an air-circulated oven at 105 °C to remove moisture, and a minimum of three samples were tested and the average values are reported in the next section.

The crystallinity index,  $I_c$ , was determined by X-ray diffraction in a RIGAKU Rotaflex model Ru-200B diffractometer operating at 40 kV, 20 mA, and  $\lambda$  (Cu K $\alpha$ ) = 1.5406 Å. The crystallinity index was calculated using the Buschle–Diller and Zeronian equation [24]:

$$I_c = (1 - I_1/I_2) \times 100 \quad (1)$$

where  $I_1$  is the intensity at the minimum ( $18^\circ < 2\theta < 19^\circ$ ) and  $I_2$  is the intensity of the crystalline peak at the maximum ( $22^\circ < 2\theta < 23^\circ$ ).

The tensile strength of the fibers (15 mm of length and 0.5 mm of diameter) was analyzed using a DMA analyzer model 2980, from TA Instruments operating at 25 °C and 1 N min<sup>-1</sup> up to 18 N. The test was carried out using individual fibers. The fibers were previously dried for 4 h in an air-circulated oven at 105 °C to remove moisture. A minimum of 30 samples were tested.

The dispersive component of the surface energy and acid–base properties of the sisal fibers and also of the tannin and TPT were analyzed by IGC, as described in previous works [10,25]. A Shimadzu GC-17A gas chromatograph equipped with a flame ionization detector was used. The columns were made from stainless steel (316) and had an internal diameter of 5.0 mm and a length of 2.0 m. The fibers were chopped to approximately 1 mm and packed into the column. The injector and detector temperatures were maintained at 150 °C and the column at 30 °C. The flow rate of the carrier gas (N<sub>2</sub>) was 30 mL min<sup>-1</sup>. The TPT was previously triturated using an analytical mill (IKA-Labortechnik, model A-10) and sifted through mesh 60–150 and then, packed into the column. For the analysis, the injector and detector temperatures were maintained at 150 °C and the column at 50 °C. Before each analysis, the columns packed with the samples were conditioned overnight at 150 °C with N<sub>2</sub> flow of 50 mL min<sup>-1</sup> to remove traces of water and volatile contaminants. In order to work at infinite dilution conditions, very small amounts (0.1 mL) of probes were injected with a gas-tight Hamilton micro-syringe. The non-polar probes consisted of a series of n-alkanes from pentane to decane (Sigma–Aldrich), with methane as a marker, and the polar probes were tetrahydrofuran (Sigma–Aldrich) and chloroform (Sigma–Aldrich). At least three individual injections were made for each probe, and the reliability of the trials was very good for all measurements.

The following thermodynamic relation was used to determine the London component of the surface free energy of the materials:

$$RT \ln V_n = 2N(\gamma_S^d)^{1/2} a(\gamma_L^d)^{1/2} \quad (2)$$

where  $V_n$  is the retention volume,  $N$  is Avogadro's number,  $a$  is the surface area of the probe molecule,  $\gamma_L^d$  is the dispersive component of the surface free energy of the probe in liquid state,  $R$  is the gas constant, and  $T$  is the absolute temperature of the column.

The acid–base properties of the surfaces can be obtained from the equation:

$$\Delta G_A^{SP} = NaW_A^{SP} = RT(\ln V_n / \ln V_{n,ref}) \quad (3)$$

where  $\Delta G_A^{SP}$  is the free energy of adsorption,  $V_n$  is the retention volume of the polar probe under consideration, and  $V_{n,ref}$  is obtained from the  $n$ -alkane reference line, at the appropriated  $(\gamma_L^d)^{1/2}$  value. The  $\Delta G$  value is determined for each probe and the obtained values are considered to describe the acid ( $AN_S \equiv \Delta G_A^{SP_{donor}}$ ) and basic ( $DN_S \equiv \Delta G_A^{SP_{acceptor}}$ ) properties of the surface. The value of the ratio  $AN_S/DN_S$  can be taken as an indication of the predominance of acid ( $AN_S/DN_S \geq 1.1$ ) or basic ( $AN_S/DN_S \leq 0.9$ ) sites at the interface under investigation. In this arbitrary scale, amphoteric and neutral (non-polar) surfaces are related to  $AN_S/DN_S$  values in the range of 0.9–1.1 and near 0, respectively [26,27].

#### 2.4.3. Thermosets and composites

The Izod impact strength was assessed using Izod impact CEAST Resil 25 equipment. Twenty unnotched samples were cut from each plate and shaped according to the ASTM D256 (63.5 mm length  $\times$  12.7 mm width  $\times$  4.5 mm thickness). The impact tests were carried out at room temperature with an impact speed of 4 m s<sup>-1</sup> and incident energy of 5.5 J.

The SEM images were taken with a Zeiss–Leica apparatus, model 440, with an electron acceleration of 20 kV. Fractured samples were covered with a thin layer of gold in a sputter-coating system prior to analysis.

The dynamic mechanical thermoanalysis was carried out using a DMA thermal analyzer, model 2980 from TA Instruments, operating with the 3-point bending clamp (flexural mode), oscillation amplitude of 20  $\mu$ m, frequency of 1 Hz, heating rate of 2 °C min<sup>-1</sup>, and temperature in the range of 30–230 °C. The equipment was calibrated with a metallic standard. The composites samples dimensions were 64 mm of length  $\times$  12 mm of width  $\times$  3.2 mm of thickness. A minimum of three samples were tested.

The water absorption analyses were performed according to the ASTM D570. The samples (76.2 mm  $\times$  25.4 mm  $\times$  3.2 mm) were immersed in distilled water at room temperature. After certain intervals, they were removed from water, put in a piece of dry cloth (only to remove the excess of water), and weighed on a high-precision balance. The percentage of mass increase (water content) was calculated by the weight difference. A minimum of two samples were tested.

## 3. Results and discussion

### 3.1. Characterization of the tannin and tannin–phenolic resin

The FT-IR spectra of the tannin and the tannin–phenolic resin (figures not shown) showed a wide and intense band in the region between 3100 and 3500 cm<sup>-1</sup> related to the –OH stretching and deformation of the alcohol and phenol groups. A weak band observed around 2900 cm<sup>-1</sup> is related to the –C–H axial deformation. In the resin this band is enlarged because of the –CH<sub>2</sub>–OH groups introduced during the hydroxymethylation of the phenolic rings (structure shown in Fig. 1). The bands observed between 1620 and 1450 cm<sup>-1</sup> are related to C=C axial deformation of the aromatic rings [28]. The bands between 1350 and 1230 cm<sup>-1</sup> are associated to the C–O–C axial deformation. Around 1010 and 1030 cm<sup>-1</sup>, it was observed a band related to the –C–OH stretching. In the resin spectrum, this band is widened due to the larger quantity of these bonds present in the hydroxymethyl groups (–CH<sub>2</sub>OH). Less intense bands were observed between 800 and 700 cm<sup>-1</sup>, which are related to the C–H angular deformation outside the plane in aromatic rings [29]. The absence of a band around 1740 cm<sup>-1</sup>, which is characteristic of C=O bond in carboxyl group, confirms that the tannin used in this work is a condensed-type tannin. The FT-IR spectrum of hydrolysable tannins shows that this band is due to the ester bond present in its structure [29].

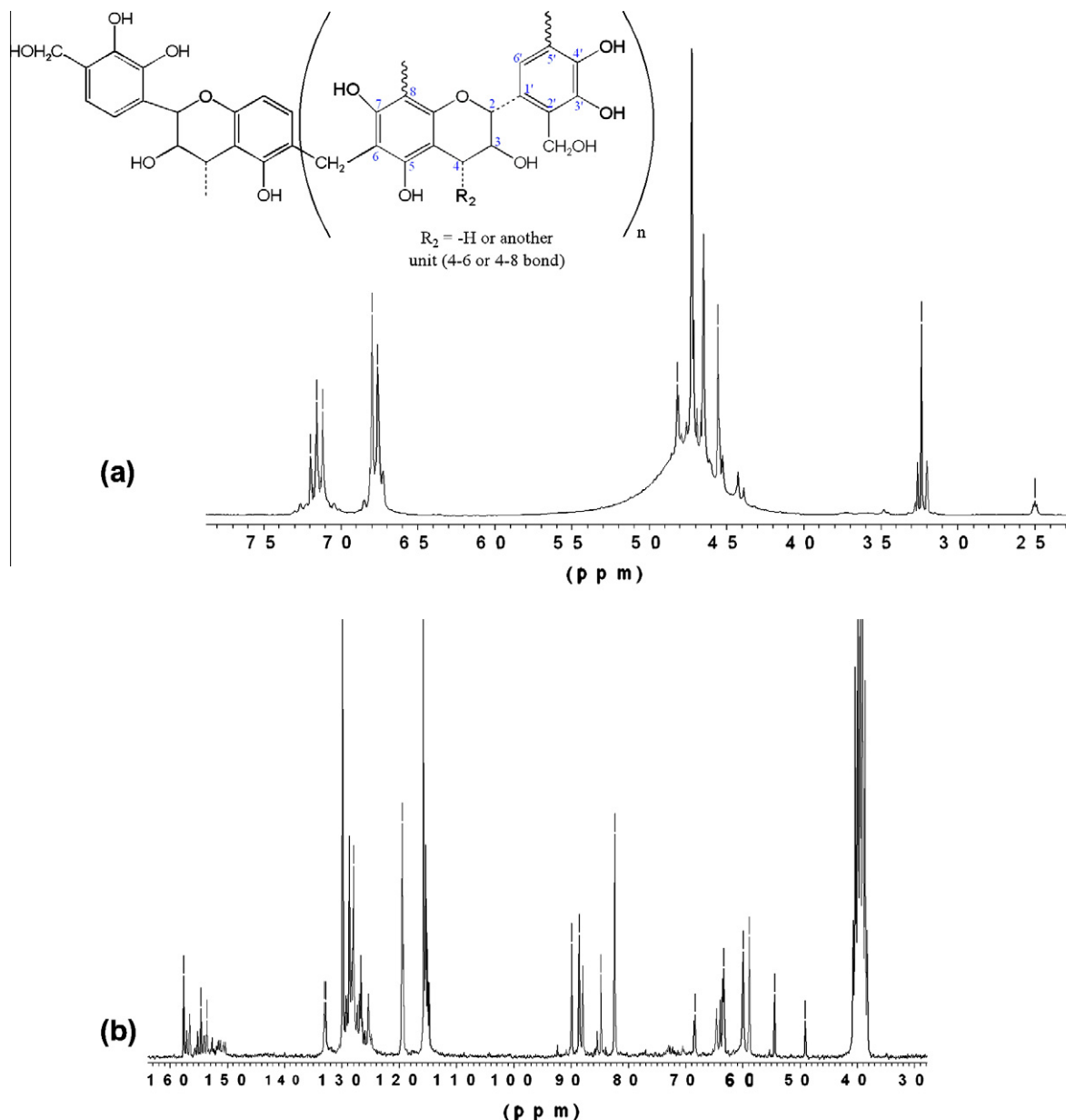


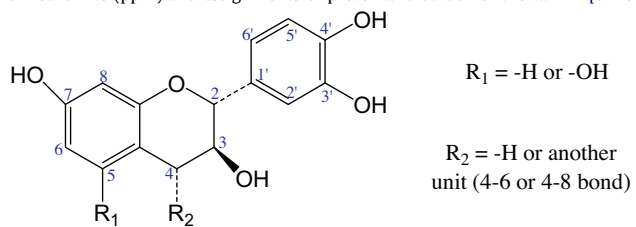
Fig. 1. NMR spectra of the tannin-phenolic resin: (a) <sup>1</sup>H (solvent: DMSO-d<sub>6</sub>, 512 scans); (b) <sup>13</sup>C (solvent: DMSO-d<sub>6</sub>, 16,800 scans).

Table 1 shows the peaks assignments of the <sup>1</sup>H and <sup>13</sup>C NMR spectra of the tannin (figures not shown). The analysis of the NMR spectra also confirms that it is a condensed-type tannin, with condensed rings and carbon-carbon bonds interconnecting the rings. The <sup>13</sup>C NMR spectrum of the hydrolysable tannin must present a characteristic ester carbon signal, because in this tannin, the rings are interconnected by ester-type bonds [30]. In the region between 60 and 84 ppm of the <sup>13</sup>C NMR spectrum, several signals related to the carbons of polymeric and monomeric carbohydrates was observed, which are always present in industrial tannins [31]. These peaks can mask the peaks of the carbons C<sub>3</sub> and C<sub>2</sub> of the tannin.

<sup>1</sup>H and <sup>13</sup>C NMR spectra of the tannin-phenolic resin are shown in the Fig. 1. In the <sup>1</sup>H spectrum, a very intense peak at 4.7 ppm was observed, which is a characteristic of protons of hydroxymethyl groups linked to aromatic ring. The peak at 3.2 ppm is related to the proton linked to carbon 4, with R<sub>2</sub> = H. The peak at 4.5 ppm is related to the proton linked to carbon 2, and the peak

at 4.8 ppm is related to the proton linked to carbon 2 with R<sub>2</sub> = another unit. In the region of aromatic protons, two sets of peaks were observed, between 6.7 and 7.1 ppm, corresponding to higher chemical shifts when compared with the tannin. These peaks are related to the aromatic protons of tannin and to the phenol hydroxymethylated rings linked by methylene bridges generating the tannin-phenolic resin. In the <sup>13</sup>C NMR spectrum of the tannin-phenolic resin, the peaks at 49 and 54 ppm are related to the introduction of -CH<sub>2</sub> groups linked to aromatic rings. The peaks at 91 and 107 ppm of the tannin spectrum, related to six and eight carbons (*ortho* position in the aromatic ring; Table 1) are absent in the tannin-phenolic resin. This probably indicates that the reactions occurring in this position, displaces the signal of these carbons. The signals related to aromatic carbons appeared at higher chemical shifts, compared to tannin (Table 1), due to the occurrence of reactions between hydroxymethylated tannin and phenol, followed by the formation of methylene bridges, resulting in the tannin-phenolic resin.

**Table 1**  
Chemical shifts (ppm) and assignments of proton and carbon of the tannin [31–33].



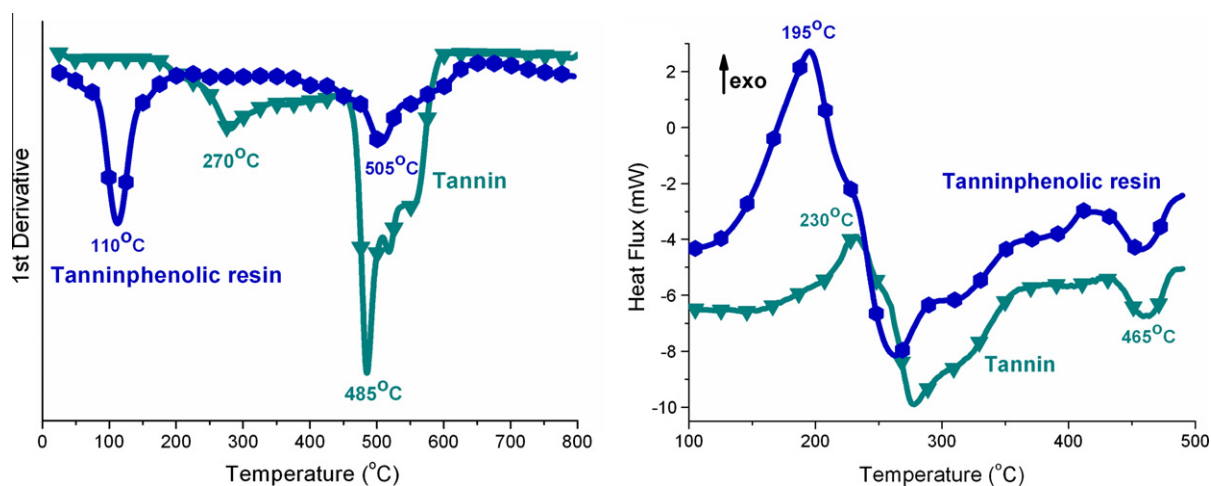
Chemical shifts (ppm)	Assignments
<sup>1</sup> H	
3.1	H <sub>4</sub> , when R <sub>2</sub> = -H
3.4–3.6	H <sub>3</sub> and residual carbohydrates
4.3–4.4	H <sub>2</sub>
4.8	H <sub>4</sub> , when R <sub>2</sub> = other unity linked by C <sub>6</sub> or C <sub>8</sub>
6.2–6.8	Aromatics protons
8.4	Protons of the -OH groups
<sup>13</sup> C	
29	C <sub>4</sub> when R <sub>2</sub> = -H
43	C <sub>4</sub> when R <sub>2</sub> = other unity linked by C <sub>6</sub> or C <sub>8</sub>
60–84	C <sub>3</sub> , C <sub>2</sub> and residual carbohydrates
91–107	C <sub>6</sub> and C <sub>8</sub>
115	C <sub>2'</sub> and C <sub>5'</sub>
118	C <sub>6'</sub>
130	C <sub>1'</sub>
133	C <sub>4'</sub>
145	C <sub>3'</sub>
155–156	C <sub>5</sub> and C <sub>7</sub>

Fig. 2 show the first derivative of TG (dTG) and DSC curves of the tannin and tannin–phenolic resin. The tannin degradation begins around 230 °C, this event causes an exothermic peak in the DSC curve (Fig. 2b), and a peak with a maximum at 270 °C in dTG curve (Fig. 2a). The maximum of the tannin degradation is observed at 485 °C, involving the aromatic rings decomposition, which generates an endothermic peak at 465 °C in the DSC curve (Fig. 2b) due to the vaporization of volatiles. The peak of mass loss observed at 110 °C in the dTG curve of the tannin–phenolic resin (Fig. 2a) is related to condensation stages of the pre-polymer, which occur during the scanning and that is accompanied by the release of water. These reactions may represent reactions between short chains, generating longer chains and/or the beginning of the cross-linking reactions (cure). In the DSC curve, this event causes an exothermic peak around 195 °C (Fig. 2b). The peak around 500 °C corresponds to the mass loss due to the decomposition of

the thermoset formed during the scanning, involving the aromatic rings decomposition.

### 3.2. Characterizations of the sisal fiber, TPT and TPC

The sisal fibers used as reinforcement in the composites were previously characterized (8.0% ± 0.3 of moisture; 1.3% ± 0.1 of ash) and, such as all lignocellulosic fibers, is composed mainly of cellulose (64.4% ± 1.1, free of moisture), hemicellulose [23.9% ± 0.4, determined as difference between holocellulose (cellulose + hemicellulose) and cellulose content] and lignin (9.7% ± 0.3, free of moisture). The high cellulose content and the high crystallinity (60.6%) of the sisal fibers, when compared to other lignocellulosic fibers, provide their good mechanical properties, as its tensile strength (288 ± 32 MPa). The coir fibers, characterized and used in a companion paper [23], showed lower cellulose content (43.4%), crystallinity (44%), and tensile strength (120 MPa), compared to sisal fibers. Thus, the improved properties of sisal fibers can lead to composites with better mechanical properties compared to those reinforced with coir fibers. The sisal fibers were also characterized by IGC, and the obtained results are shown in Table 2. The stronger the interaction between the sample and the apolar volatile probe, the greater will be the slope  $\gamma_5^d$  of the reference line, the liquid retention volume  $V_n$  (Eq. (2)) and the column retention time  $t_R$  (Eq. (2)). In this context, a high value of  $\gamma_5^d$  can be considered as an indication of a high number of non-polar sites on the surface of the material [25]. The sisal fibers presented a higher value of the dispersive component ( $\gamma_5^d = 49.3 \text{ mJ m}^{-2}$ ), when compared with previous results [10]. However, it must be pointed out that the sisal used in the present study was received from other supplier and has contents of lignin and holocellulose (hemicellulose + cellulose) different from the previous one. Agroclimatic conditions, such as soil properties, air humidity, temperature, and solar radiation, can affect the growth, structure, chemical compositions, and consequently, the surface parameters of vegetable fibers. Mills et al. [34] found a value of  $38.4 \text{ mJ m}^{-2}$  for sisal (at 30 °C, as in the present study), but the composition of the fiber is not mentioned. The high value of the dispersive component of the sisal used in the present study can be taken as an indication that the surface analyzed is rich in lignin, which presents multiple aromatic rings, contributing to the high density of apolar groups in the fiber surface. It was also observed a slight predominance of acid sites, considering the higher values of  $AN_5$  compared to  $DN_5$ , resulting in a surface with general acid character ( $AN_5/DN_5 = 1.1$ ), as already observed in a previous study [10].



**Fig. 2.** (a) dTG curves and (b) DSC curves of the tannin and tannin–phenolic resin synthetic air atmosphere (20 mL min<sup>-1</sup>) and heating rate of 10 °C min<sup>-1</sup>.

**Table 2**

Dispersive component of surface free energy ( $\gamma_S^d$ ) and acid–base ( $AN_S$ ,  $DN_S$ ) properties of the sisal fibers, phenolic (phenol–formaldehyde) thermoset, tannin–phenolic thermoset, and tannin.

	$\gamma_S^d$ (mJ m <sup>-2</sup> )	$AN_S$	$DN_S$	$AN_S/DN_S$
Sisal fibers	49.3	5845	5396	1.1
Phenolic thermoset	34.2	5104	3473	1.5
Tannin–phenolic thermoset	39.1	9043	2940	3.1
Tannin	38.4	6826	3738	1.8

The IGC was also used to characterize the tannin and the thermoset matrices. To our knowledge, this characterization of tannin is unprecedented. The tannin presented a value of the dispersive component ( $\gamma_S^d = 38.4$  mJ m<sup>-2</sup>, Table 2) that can be taken as an indication of considerable concentration of apolar sites, probably mainly due to the high proportion of aromatic rings and non-aromatic condensed rings present in its structure. The value of  $AN_S$  of tannin surface was almost two times higher than  $DN_S$ , which demonstrates that tannin has a surface with predominance of acid sites ( $AN_S/DN_S = 1.8$ ), a consequence mainly of the high amount of hydroxyl groups in its structure. The TPT presented higher value of the dispersive component ( $\gamma_S^d$ ) and, therefore, more apolar character compared to phenolic (phenol–formaldehyde) thermoset (Table 2), as a consequence of the presence of tannin, which has a high proportion of aromatic rings and non-aromatic condensed rings in its structure as already mentioned. The value of  $AN_S/DN_S$  of the TPT was superior to that presented by phenolic thermoset (Table 2), demonstrating that the TPT has a surface with more acid character. The increase in the acid character is probably due to the higher accessibility of the probes to the acid sites, mainly hydroxyl groups, present in large quantities in condensed tannins and, therefore, in the TPT. The TPT showed the dispersive component value ( $\gamma_S^d = 39.1$  mJ m<sup>-2</sup>, Table 2) closer to those of the sisal fibers used in the present study ( $\gamma_S^d = 49.3$  mJ m<sup>-2</sup>, Table 2), when compared with phenolic thermoset ( $\gamma_S^d = 34.2$  mJ m<sup>-2</sup>, Table 2). This suggests that the fiber/TPT interactions are favored, mainly between regions of low polarity of these materials. In addition, the high value of  $AN_S$  of the TPT indicates that a large number of groups with acid character were accessible for interactions with the probe and were probably accessible for interactions, via hydrogen bonding, with the sisal fibers used as reinforcement in this matrix, improving the properties of the obtained composites.

The assessment of the impact strength of the polymeric materials is a decisive factor in the selection of materials for specific application. The values of impact strength represent the total capacity of the material absorb the impact energy. Fig. 3 shows the results of Izod impact strength test of the TPT and TPC

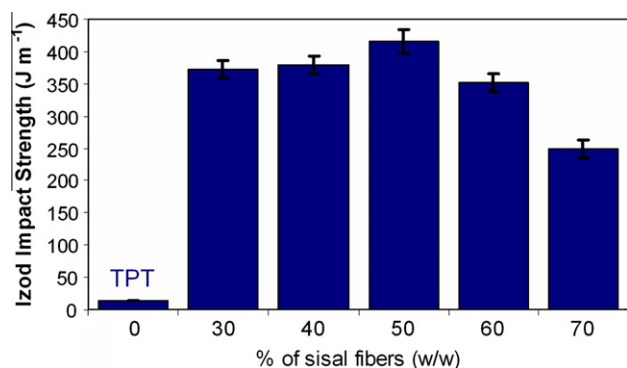


**Fig. 3.** Izod impact strength and standard deviation of the tannin–phenolic thermoset (TPT) and composites (TPC) reinforced with sisal fibers (unnotched samples).

reinforced in the range of 30–70 wt% by randomly distributed sisal fibers (3 cm of length, aspect ratio near 140). TPT (unreinforced) showed low impact strength, due to its high cross-linking. When the thermoset is reinforced, the same polymer chain can interact with several units of the reinforcement agent (fibers). If some linkage of this segment breaks due to the impact, the load is transferred to many other segments, increasing the impact strength of the material. The introduction of sisal fibers resulted in a significant improvement in the impact strength of the composites compared with the thermoset, in other words, the energy required to break the samples was higher, showing that the fibers really act as reinforcement in the composites. In the present study, many composites samples showed the “fiber bridging” mechanism. In this mechanism, not all fibers are fractured during the impact, that is, some fibers remain forming a “bridge” between the two parts of the fractured matrix. In this mechanism, part of the load applied in the matrix is transferred to the fibers, which deform, increasing the impact strength of the composite [35].

The increase in the proportion of sisal fiber used as reinforcement in the TPC, up to 50 wt%, enhanced the Izod impact strength, although the standard deviations approach the values (Fig. 3). Proportions of sisal fiber above 50 wt% led to a decrease in the impact strength of the composites (Fig. 3). Normally, composites prepared from thermoset matrix reinforced with vegetable fibers show improvement in their mechanical properties with the increase of proportions of fibers used as reinforcement. However, after a limit, which depends on both the matrix and the vegetable fiber types, the mechanical properties can decrease with the increase in the proportion of fibers. This is owing to the higher fiber–fiber contact that can occur, in addition to the incomplete impregnation of the fibers by the polymeric matrix. The impregnation stage of the fibers by the matrix is decisive to obtain composite with good mechanical properties. The higher fiber volume hinders the impregnation, generating regions with fiber agglomeration, intensifying the fiber–fiber interactions. The fiber agglomeration makes the material less homogeneous, resulting in a lower value of impact strength [36].

Based on the results of Izod impact strength (Fig. 3), it can be considered that in the TPC, the mass proportions of 50 wt% of sisal fiber are the limit proportion of this fiber in the composite. The increase in the proportion of fibers, above this limit of 50 wt%, probably result in a composite with large number of flaws or voids, non-homogeneous distribution of the fibers in the matrix and non-intense interactions in the interface due to poor impregnation of the fiber by the matrix, thus decreasing the impact strength of the obtained composite.

In the TPC reinforced with coir fibers, prepared in the companion paper [23], it was observed that the composite reinforced with 60 wt% of coir fiber showed the highest impact strength, 95.5 J m<sup>-1</sup>. This result shows that the optimization of the parameters of the pre-polymer synthesis, associated with choosing a fiber with higher tensile strength led to a significant improvement in the mechanical properties of the composite. TPC reinforced with 50 wt% of sisal fiber, which showed the best result among the composites prepared in the present work, showed impact strength of 416 J m<sup>-1</sup>, which corresponds to the impact strength four times greater than that of the composite reinforced with coir fiber.

Fig. 4 shows the SEM images of the fractures of the TPC reinforced with 40, 50, and 70 wt% of sisal fiber. The composites reinforced with up to 50 wt% of sisal fibers presented a good interaction in the fiber/matrix interface, as shown in the SEM images (Fig. 4a–d). In these composites, the tips of the fibers were filled by the matrix (Fig. 4a). This is important, since unfilled tips can act as stress concentrators, decreasing the mechanical properties of the composite. The fibers were uniformly distributed in the matrix (Fig. 4b), allowing a load transfer from the matrix to the

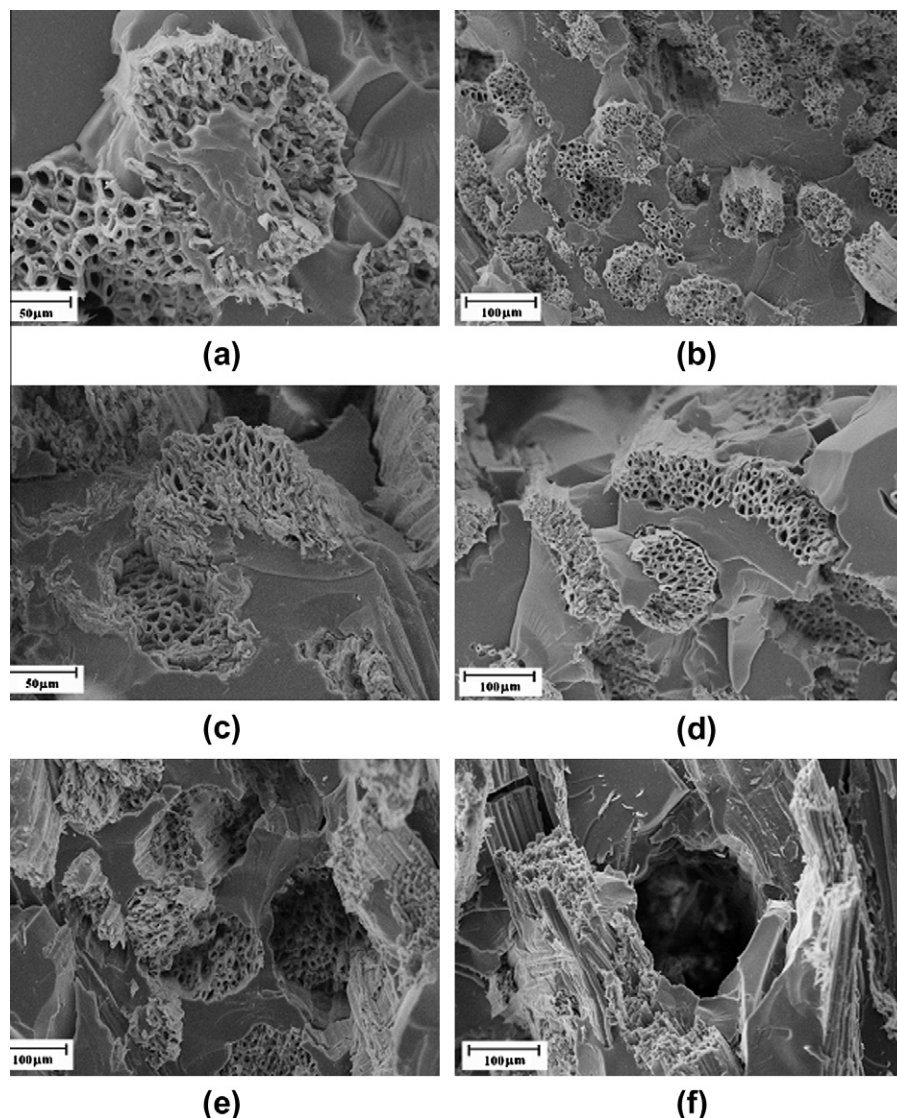


**Fig. 4.** SEM images of impact fractured surfaces of tannin-phenolic composites (TPC) reinforced with sisal fibers. (a and b) 40 wt% of sisal fibers: fiber/matrix interface and fibers uniformly distributed in the matrix; (c and d) 50 wt% of sisal fibers: fiber/matrix interface; (e and f) 70 wt% of sisal fibers: fiber/matrix interface and fibers pulled-out.

fiber more efficient and more homogeneous throughout the composite. In some regions of these composites, the fibers were well adhered to the matrix and were broken with the matrix during the Izod impact test (Fig. 4c). In other regions, the presence of cracks around the fibers (Fig. 4d) was observed, which indicates the transfer of the load applied during the impact test from the matrix to the fibers. When a load is applied on the composite, a crack is created at the point of impact. This crack propagates through the matrix and around the fibers. In this way, the energy involved in the crack propagation is distributed and absorbed by the fibers. Thus, the energy of the impact is absorbed through partial rupture of the interactions between fiber and matrix in the interface region, which release the fiber, increasing the impact strength [37].

TPC reinforced with 60 and 70 wt% of sisal fibers showed fiber agglomeration, due to the high proportion of fibers that decrease the impregnation of these fibers by the matrix. This fiber agglomeration increases the fiber-fiber contact and creates flaws in the interface (Fig. 4e), which reduces the efficiency of load transfer between the matrix and the sisal fibers, reducing the impact strength of these composites (Fig. 3). The fibers were less adhered to the

matrix, so, they were more easily pulled out during the Izod impact test (Fig. 4f).

Fig. 5a and b presents, respectively, the curves of the storage modulus ( $E'$ ) and loss modulus ( $E''$ ) versus temperature of the TPT and TPC reinforced with 30–70 wt% of sisal fibers. The storage moduli of the composites were higher than that of the thermoset (Fig. 5a), which means that the incorporation of sisal fiber in the polymeric matrix resulted in the increase of the material stiffness. For the initial temperature of analysis (25 °C), the storage moduli of the composites increased with the increase of sisal fiber proportion, from 30 to 60 wt% (Fig. 5a). As the sisal fiber shows high content of cellulose (64.4%) and crystallinity (60.6%), the modulus of the sisal fiber is superior to the tannin-phenolic matrix. Thus, as the portion of fibers increased, the modulus of the composite also increased. The exception from this behavior was observed for the composite reinforced with 70 wt% of sisal fiber. This composite showed storage modulus smaller than expected, considering only the effect of hardening caused by the sisal fibers. The low value of  $E'$  in the composite reinforced with 70 wt% of fiber is probably due to the dissipation of energy in the transfer of load in the

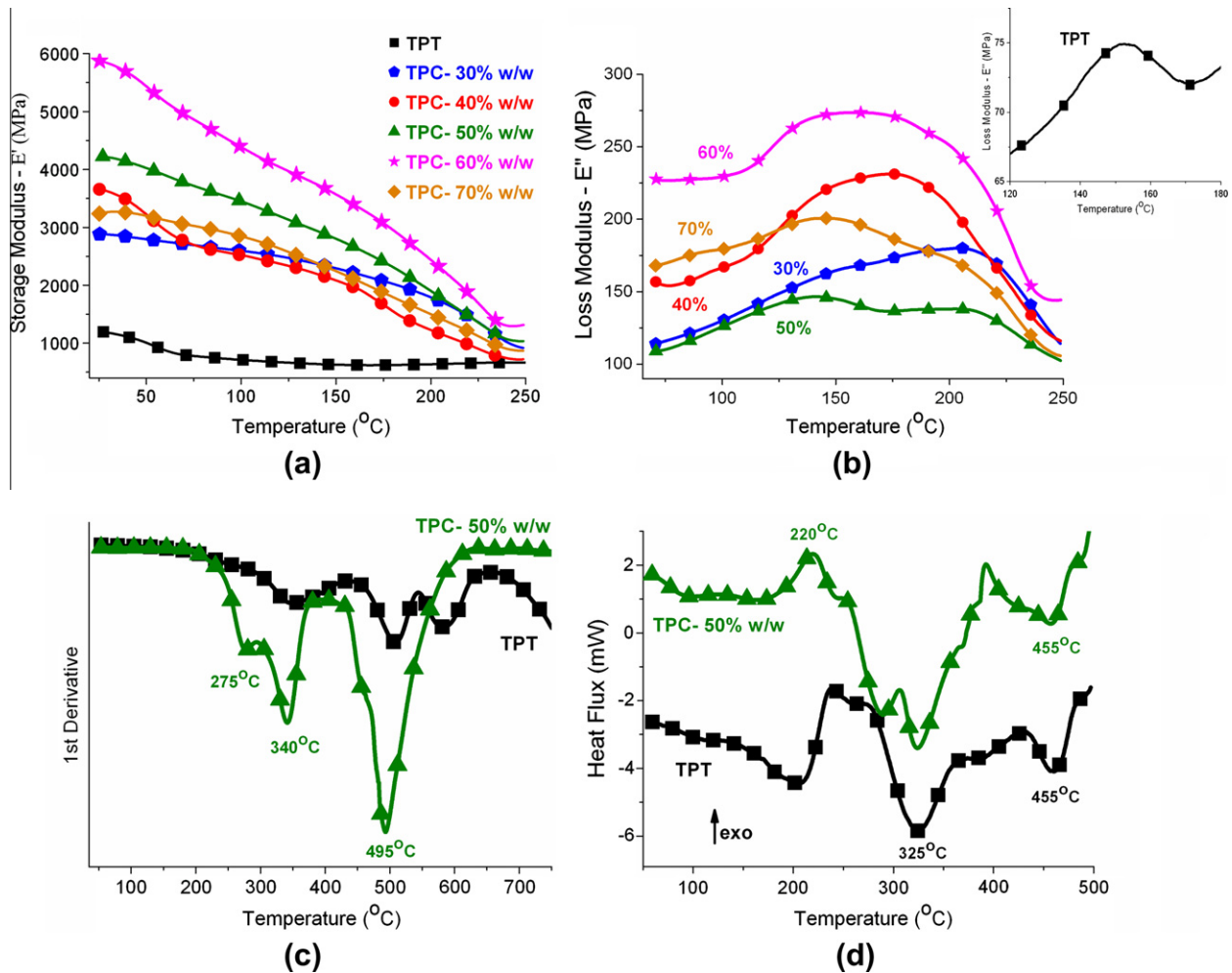


**Fig. 5.** (a)  $E'$  versus temperature curves of the tannin–phenolic thermoset (TPT) and composites (TPC) reinforced with sisal fibers; (b)  $E''$  versus temperature curves (TPT above, on the right); (c) dTG curves and (d) DSC curves.

interface. This dissipation of energy occurs due to the weak fiber/matrix interface in this composite, caused by the difficulty of impregnation of the large amount of fiber, as mentioned previously.

The composites reinforced with 30 and 50 wt% of sisal fibers showed the lowest loss moduli (Fig. 5b) confirming the good interaction in the fiber/matrix interface in these composites, as previously observed by the SEM images (Fig. 4) and by the results of the impact test (Fig. 3). The composites reinforced with higher proportions of fibers showed higher loss moduli, probably due to the large number of flaws present, as for instance points of tension, fiber bending, microcracks and voids. These flaws contribute to a higher dissipation of energy through friction [38]. The increase in the proportion of fibers used as reinforcement, above 50 wt%, hindered the impregnation of the fibers by the matrix, resulting in the production of more flaws and voids, responsible for increasing  $E''$  and reducing the Izod impact strength (Fig. 3).

The enlargement of the peaks observed in  $E''$  curves of the composites when compared with the thermoset (Fig. 5b) indicated that the composites reinforced with sisal fibers had heterogeneous structure, with regions of diversified cross-linking density [4,39]. Increased volumes of fibers mean lower volume of matrix. During the cross-linking, the diffusion of the pre-polymer chains for the establishment of cross links becomes more difficult, probably resulting in a less homogeneous material, in terms of cross-linking density. Moreover, the chains closer and more distant of the

interface can have different behaviors, which also leads to the enlargement in the peaks of  $E''$ .

Although the thermoset matrix presents a cross-linked structure, the cross-linking is not total, allowing the movement of chain segments between the cross-linking points. Thus, using the maximum of the  $E''$  curve, it was possible to determine the glass transition temperature ( $T_g$ ) of these materials (Fig. 5b). The  $T_g$  of the TPT was observed at 152 °C, while the  $T_g$  of the TPC composites occurred around 175 °C. This higher value of  $T_g$  in the composites was due to the presence of the fibers that hinder the movement of the chain segments at the fiber/matrix interface, displacing the glass transition of these materials to higher temperatures when compared to the thermoset.

Fig. 5c and d shows, respectively, the first derivative of TG (dTG) and DSC curves of the TPT and TPC reinforced with 50 wt% of sisal fiber. The other composites showed similar thermal behavior (curves not shown). In the dTG curves of the composites (Fig. 5c) around 275 °C, it was observed a peak of mass loss probably due to the volatilization of water generated in stages of residual cure occurred during the scanning, in addition to the decomposition of hemicellulose of the sisal fibers and the tannin of the matrix. At 340 °C, the peak of mass loss is related to the beginning of the thermal decomposition of the cellulose present in the sisal fibers. The last stage of mass loss has the maximum of the peak around 500 °C and is related to the decomposition of the polymeric chains



and the aromatic rings of the matrix, in addition to the decomposition of the lignin present in the sisal fibers, explaining the peak more intense in the composites compared to the thermoset.

In the DSC curves (Fig. 5d) around 220 °C, an exothermic peak related to the residual cure and/or the decomposition of the hemicellulose was observed. Around 325 °C, an endothermic peak due to the release of volatiles generated by oxidative process was observed, in addition to the decomposition of the cellulose present in the sisal fibers in the composite. The decomposition reactions are exothermic, but as at the same time, the release of volatiles occurs (endothermic event), the peak observed can be exothermic or endothermic, depending on the balance between the decomposition reactions and release of volatiles. At 455 °C, another endothermic peak was observed, related to the decomposition of the lignin in the sisal fibers, polymeric chains, and aromatic rings of the matrix.

Fig. 6a shows the results obtained in the water absorption test of the TPT and composites (TPC) reinforced with 30 and 70 wt% of sisal fibers. The water absorption of the composites reinforced with 40, 50, and 60 wt% of sisal fibers has values between the two composites presented. As the sisal fibers have hydrophilic character, the increase in the portion of fiber used as reinforcement intensifies the process of water absorption in the composites, increasing the water absorbed by the composites, as the amount of fibers increases (Fig. 6a). Thus, the hydrophilic nature of the sisal fibers, with polar groups in their surface that interact easily with

the water molecules, is the mainly responsible for the water absorption in the composites. In the fiber composition, the hemicellulose is considered the main responsible for the water absorption, although not crystalline cellulose and lignin also play an important role in this process.

The presence of higher amount of fiber in the composites can interfere in the cure process of the matrix, and the degree of the matrix cross-linking also interferes in the process of water absorption in the composites. The lower cross-linking density in the polymeric matrix facilitates the penetration of water molecules in the matrix network, increasing the water absorption in the composite.

The mechanism involved in the process of water diffusion in the TPT and TPC was evaluated according to the Fick's law, as described in previous work [2,11]. The introduction of the sisal fibers in the composites caused a significant increase in the affinity of the composite by the water molecules, determined by the parameter  $k$ , which increased from 0.1 (thermoset) to 0.6–0.7 (composites). Thus, the results indicate that the affinity of the sisal fibers by water molecules is considerably higher than the affinity of the tannin–phenolic matrix by the water. Considering the variation of the proportion of sisal fibers used as reinforcement, a significant change in the values of  $k$  was not observed. This result shows that the affinity of the material by the water is governed mainly for the chemical nature of the components of the composite, being more dependent on the chemical nature of the fibers used as reinforcement. As in this study, the chemical nature of the fibers was not changed, the parameter  $k$  for the composites is almost the same.

The composites reinforced in the range of 30–50 wt% of sisal fibers showed values of the diffusion coefficient ( $D$ ) (Fig. 6b) close to that of thermoset (without fiber reinforcement). The diffusion coefficient defines the ability of the water molecules in penetrate in the composites, so that the higher the value of  $D$ , the faster the diffusion of water molecules inside the material. The tannin–phenolic matrix has a high proportion of hydroxyl groups that can interact with water molecules via hydrogen bonds. Thus, the introduction of sisal fibers up to 50 wt% did not change the rate of diffusion of the water molecules inside the composites.

In the composites reinforced with 60 and 70 wt% of sisal fibers, a large increase in the value of  $D$  was observed. This considerable increase occurred due to the presence of flaws, mainly in the fiber/matrix interface, which behave as “free spaces” for the diffusion of water, accelerating the diffusion inside the composites. This effect was higher in the composite reinforced with 70 wt% of sisal fiber, which was the composite with higher amount of flaws in the fiber/matrix interface (Fig. 4e and f) owing to difficulty of impregnate a high amount of fiber.

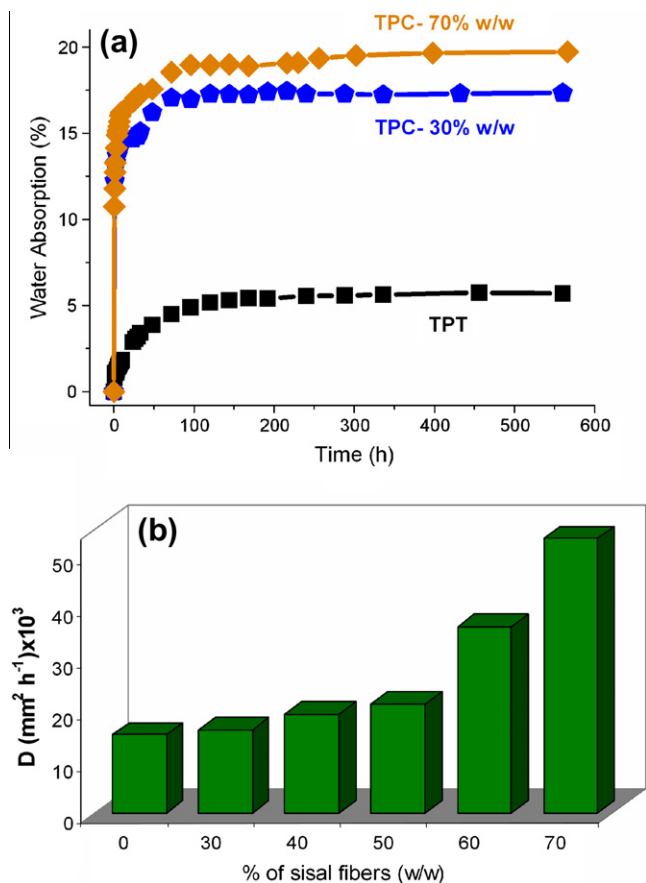


**Fig. 6.** (a) Results of water absorption test of the tannin–phenolic thermoset (TPT) and composites (TPC) reinforced with sisal fibers. The standard deviations related to the water absorption measurements ranged from 0.01% to 1.6%; (b) values of the diffusion coefficient ( $D$ ) from the linear regression curve of water absorption experiments according to the Fick's model. The standard error (angular coefficient) ranged from  $1 \times 10^{-9}$  to  $3 \times 10^{-5}$ .

#### 4. Conclusion

Tannin, obtained from natural sources, can be used as a macromonomer in the synthesis of the tannin–phenolic resins used for the production of composites. The TPT have dispersive component ( $\gamma^d$ ) closer to sisal fibers, when compared to phenolic (phenol–formaldehyde) thermoset, which suggests a better interaction in the fiber/matrix interface. The characterization of the composites showed that the increase in the proportion of sisal fibers used as reinforcement in the TPC resulted in increased Izod impact strength up to 50 wt% of sisal fibers. The increase in the proportion of sisal fibers above this limit led to composites with lower impact strength, mainly due to the difficulty of impregnate a large amount of fibers. The composite reinforced with 50 wt% of sisal fiber also had high stiffness and the lower loss modulus, confirming the good fiber/matrix interface of this composite, also observed by the SEM. It is important to highlight the high content of raw material obtained from renewable sources used in the

preparation of this composite, in which 40 wt% of tannin substituted the phenol in the preparation of the matrix and 50 wt% of matrix was replaced by sisal fibers.

### Acknowledgments

The authors gratefully acknowledge FAPESP (The State of São Paulo Research Foundation, Brazil) for the doctoral fellowship for E.C.R. and for financial support. E.F. is grateful to CNPq (National Research Council, Brazil) for the research productivity fellowship and financial support.

### References

- [1] Ku H, Wang H, Pattarachaiyakop N, Trada M. A review on the tensile properties of natural fiber reinforced polymer composites. *Compos Part B* 2011;42(4):856–73.
- [2] Ramires EC, Megiatto Jr JD, Gardrat C, Castellan A, Frollini E. Biobased composites from glyoxal-phenolic resins and sisal fibers. *Bioresour Technol* 2010;101(6):1998–2006.
- [3] Ramires EC, Gardrat C, Megiatto Jr JD, Castellan A, Frollini E. Biobased composites from glyoxal-phenol matrices reinforced with microcrystalline cellulose. *Polimeros* 2010;20(2):126–33.
- [4] Trindade WG, Hoareau W, Megiatto Jr JD, Razera IAT, Castellan A, Frollini E. Thermoset phenolic matrices reinforced with unmodified and surface grafted furfuryl alcohol sugarcane bagasse and curaua fibers: properties of fibers and composites. *Biomacromolecules* 2005;6(5):2485–96.
- [5] Ashori A. Wood-plastic composites as promising green-composites for automotive industries! *Bioresour Technol* 2008;99(11):4661–7.
- [6] Alawar A, Hamed AM, Al-Kaabi K. Characterization of treated date palm tree fiber as composite reinforcement. *Compos Part B* 2009;40(7):601–6.
- [7] Nicolai FNP, Botaro VR, Cunha Lins VF. Effect of saline degradation on the mechanical properties of vinyl ester matrix composites reinforced with glass and natural fibers. *J Appl Polym Sci* 2008;108(4):2494–502.
- [8] Mano B, Araújo JR, Spinacé MAS, De Paoli M-A. Polyolefin composites with curaua fibres: effect of the processing conditions on mechanical properties, morphology and fibres dimensions. *Compos Sci Technol* 2010;70(1):29–35.
- [9] Ramires EC, Megiatto Jr JD, Gardrat C, Castellan A, Frollini E. Valorization of an industrial organosolv-sugarcane bagasse lignin: characterization and use as a matrix in biobased composites reinforced with sisal fibers. *Biotechnol Bioeng* 2010;107(4):612–21.
- [10] Megiatto Jr JD, Silva CG, Rosa DS, Frollini E. Sisal chemically modified with lignins: correlation between fibers and phenolic composites properties. *Polym Degrad Stab* 2008;93(6):1109–21.
- [11] Megiatto Jr JD, Ramires EC, Frollini E. Phenolic matrices and sisal fibers modified with hydroxyl terminated polybutadiene rubber: impact strength, water absorption, and morphological aspects of thermosets and composites. *Ind Crop Prod* 2010;31(1):178–84.
- [12] FAO (Food and Agriculture Organization of the United Nations), 2010. <<http://www.fao.org/DOCREP/004/Y1873E/y1873e06.htm#bm06>>.
- [13] Ku H, Trade M, Nixon R, Wong P. Flexural properties of phenolic resin reinforced with glass powder: preliminary results. *J Appl Polym Sci* 2010;116(1):347–54.
- [14] Megiatto Jr JD, Silva CG, Ramires EC, Frollini E. Thermoset matrix reinforced with sisal fibers: effect of the cure cycle on the properties of the biobased composite. *Polym Test* 2009;28(8):793–800.
- [15] Iyim TB. Modification of high ortho novolac resin with diacids to improve its mechanical properties. *J Appl Polym Sci* 2007;106(1):46–52.
- [16] Wang S, Adanur S, Jang BZ. Mechanical and thermo-mechanical failure mechanism analysis of fiber/filler reinforced phenolic matrix composites. *Compos Part B* 1997;28(3):215–31.
- [17] Handique JG, Baruah JB. Polyphenolic compounds: an overview. *React Funct Polym* 2002;52(3):163–88.
- [18] Frollini E, Oliveira FB, Ramires EC, Barbosa Jr. V. Composites based on tannins: production, process and uses (portuguese), Brazil Patent BRPI0801091; 2008.
- [19] Bisanda ETN, Ogola WO, Tesha JV. Characterization of tannin resin blends for particle board applications. *Cem Concr Compos* 2003;25(6):593–8.
- [20] Peña C, Caba K, Eceiza A, Ruseckaite R, Mondragon I. Enhancing water repellence and mechanical properties of gelatin films by tannin addition. *Bioresour Technol* 2010;101(17):6836–42.
- [21] Vázquez G, González-Álvarez J, Antorrena G. Curing of a phenol-formaldehyde-tannin adhesive in the presence of wood. Analysis by differential scanning calorimetry. *J Therm Anal Calorim* 2006;84(3):651–4.
- [22] Tondi G, Pizzi A. Tannin-based rigid foams: characterization and modification. *Ind Crop Prod* 2009;29(2–3):356–63.
- [23] Barbosa Jr V, Ramires EC, Razera IAT, Frollini E. Biobased composites from tannin-phenolic polymers reinforced with coir fibers. *Ind Crop Prod* 2010;32(3):305–12.
- [24] Buschle-Diller G, Zeronian SH. Enhancing the reactivity and strength of cotton fibers. *J Appl Polym Sci* 1992;45(6):967–79.
- [25] Ass BAP, Belgacem MN, Frollini E. Mercerized linters cellulose: characterization and acetylation in N, N-dimethylacetamid/lithium chloride. *Carbohydr Polym* 2006;63(1):19–29.
- [26] Lara J, Schreiber HP. Specific interactions and adsorption of film-forming polymers. *J Coat Technol* 1991;63(801):81–90.
- [27] Belgacem MN, Gandini A. Inverse gas chromatography as a tool to characterize dispersive and acid-base properties of the surface of fibers and powders. In: *Interfacial phenomena in chromatography*. New York: Marcel Dekker; 1999. p. 41–124.
- [28] Lee WJ, Lan WC. Properties of resorcinol-tannin-formaldehyde copolymer resins prepared from the bark extracts of Taiwan acacia and China fir. *Bioresour Technol* 2006;97(2):257–64.
- [29] Özacar M, Şengil A. Effect of tannins on phosphate removal using alum. *Turkish J Eng Environ Sci* 2003;27(4):227–36.
- [30] Mueller-Harvey I. Analysis of hydrolysable tannins. *Anim Feed Sci Technol* 2001;91(1–2):3–20.
- [31] Pizzi A. *Advanced wood adhesives technology*. New York: Marcel Dekker Inc.; 1994.
- [32] Duan W, Ohara S, Hashida K, Makino R. Condensed tannins from steamed *Acacia mearnsii* bark. *Holzforchung* 2005;59(3):289–94.
- [33] Foo LY. Condensed tannins: co-occurrence of procyanidins, prodelphinidins and profisetinidins in the heartwood of *Acacia Baileyana*. *Phytochemistry* 1984;23(12):2915–8.
- [34] Mills RH, Gardner DJ, Wimmer R. Inverse gas chromatography for determining the dispersive surface free energy and acid-base interactions of sheet molding compound- part II ligno-cellulosic fiber types for possible composite reinforcement. *J Appl Polym Sci* 2008;110(6):3880–8.
- [35] Matthews FL, Rawlings RD. *Composite materials: engineering and science*. 1st ed. New York: CRC Press; 1994.
- [36] Jacob M, Thomas S, Varughese KT. Mechanical properties of sisal/oil palm hybrid fiber reinforced natural rubber composites. *Compos Sci Technol* 2004;64(7–8):955–65.
- [37] Paiva JMF, Frollini E. Sugarcane bagasse reinforced phenolic and lignophenolic composites. *J Appl Polym Sci* 2002;83(4):880–8.
- [38] Zhang Z, Klein P, Friedrich K. Dynamic mechanical properties of PTFE based short carbon fibre reinforced composites: experimental and artificial neural network prediction. *Compos Sci Technol* 2002;62(7–8):1001–9.
- [39] Cook WD, Scott TF, Quay-Thevenon S, Forsythe JS. Dynamic mechanical thermal analysis of thermally stable and thermally reactive network polymers. *J Appl Polym Sci* 2004;93(3):1348–59.